AD-A007 765

ON THE STATISTICAL ANALYSIS OF THE RADAR SIGNATURE OF THE MQM-34D

James W. Wright

Army Missile Research, Development and Engineering Laboratory
Redstone Arsenal, Alabama

31 January 1975

DISPOSITION INSTRUCTIONS

DESTROY THIS REPORT WHEN IT IS NO LONGER NEEDED. DO NOT RETURN IT TO THE ORIGINATOR.

DISCLAIMER

THE FINDINGS IN THIS REPORT ARE NOT TO BE CONSTRUED AS AN OFFICIAL DEPARTMENT OF THE ARMY POSITION UNLESS SO DESIGNATED BY OTHER AUTHORIZED DOCUMENTS.

TRADE NAMES

USE OF TRADE NAMES OR MANUFACTURERS IN THIS REPORT DOES NOT CONSTITUTE AN OFFICIAL INDORSEMENT OR APPROVAL OF THE USE OF SUCH COMMERCIAL HARDWARE OR SOFTWARE.

UNCLASSIFIED

SECURITY CLASSIFICATION OF THIS PAGE (When Data Entered)

REPORT DOCUMENTATION PAGE

READ INSTRUCTIONS BEFORE COMPLETING FORM

1. REPORT NUMBER
Technical Report RE-75-13

2. GOVT ACCESSION NO.

3. RECIPIENT'S CATALOG NUMBER
AD-A-007 765

4. TITLE (and Subtitle)
ON THE STATISTICAL ANALYSIS OF THE RADAR SIGNATURE OF THE MQM-34D, INTERIM REPORT NUMBER TWO

5. TYPE OF REPORT & PERIOD COVERED

6. PERFORMING ORG. REPORT NUMBER

7. AUTHOR(s)
James W. Wright

8. CONTRACT OR GRANT NUMBER(s)

9. PERFORMING ORGANIZATION NAME AND ADDRESS
Commander, US Army Missile Command
Attn: AMSMI-RE
Redstone Arsenal, Alabama 35809

10. PROGRAM ELEMENT, PROJECT, TASK AREA & WORK UNIT NUMBERS
DA Project No. 1X364307D212
AMCMS Code No. 634307.12.17100

11. CONTROLLING OFFICE NAME AND ADDRESS

12. REPORT DATE
31 January 1975

13. NUMBER OF PAGES
27

14. MONITORING AGENCY NAME & ADDRESS (if different from Controlling Office)

15. SECURITY CLASS. (of this report)
UNCLASSIFIED

15a. DECLASSIFICATION/DOWNGRADING SCHEDULE

16. DISTRIBUTION STATEMENT (of this Report)

Approved for public release; distribution unlimited.

17. DISTRIBUTION STATEMENT (of the abstract entered in Block 20, if different from Report)

18. SUPPLEMENTARY NOTES

19. KEY WORDS (Continue on reverse side if necessary and identify by block number)

Radar cross section
Glint
Monostatic and bistatic conditions
Vertical polarization
Near broadside aspects
Near nose-on aspects

20. ABSTRACT (Continue on reverse side if necessary and identify by block number)

This report contains the results of an analysis of the radar signature of the MQM-34D target drone for aspect angles near normal to the roll axis for a vertically polarized measurements system. The radar cross section and glint are analyzed for monostatic and bistatic conditions and are compared with classical models. The glint is larger for near broadside aspects than for near nose-on aspects, as expected. The radar cross section does not roll off with increasing bistatic angle for these aspects as it does for near nose-on aspects.

CONTENTS

INTRODUCTION

The purpose of this report is to present some preliminary results of the statistical analysis of the RATSCAT measurements of the radar scattering of the MQM-34D (BQM-34A) target drone. The raw data from RATSCAT are reported in graphical form in an AFSWC three-volume report.[1]

The results reported here are a statistical analysis of the radar signature for two sets of data near normal to the roll axis (near broadside) for monostatic and bistatic conditions and vertical polarization. The radar cross section (RCS) is compared with three classical statistical models, and the glint is compared with a normal distribution.

An analysis of two sets of data near nose-on aspects was reported in Technical Report RE-75-7.[2]

MEASUREMENTS CONDITIONS AND DATA SELECTION

Sixteen combinations of roll and pitch values were used in the set of measurements. These 16 cuts are all combinations of four roll angles (0°; 30°; 60°; 90°) and four pitch angles (0°; 10°; 20°; 30°). For each cut, monostatic and bistatic (10°; 20°; 30°) measurements were made for vertically polarized (VV), horizontally polarized (HH), and cross polarized (VH) antenna configurations. The monostatic measurements were very extensive, including full polarization scattering matrix (RCS and phase) and glint for each polarization. Due to the width of the glint spikes, the data were taken at 0.01° intervals. At 10° and 20° bistatic angles, only the RCS was taken, the measurement interval being increased to 0.1°. At 30° bistatic angle, the RCS and glint were measured, the measurement interval being 0.1°.

The aspect angles for the cuts of data are plotted in Figure 1. The aspect angles are defined to be the polar angles measured from nose-on to the target. The bounds on theta are $\pm 180^\circ$ and the bounds on phi are -90° to 90°. It is obvious from the plots that the measurements were not taken uniformly over the solid angle coverage available; but, if the target is assumed to be symmetrical in theta, a useful analysis can be achieved. The aspect angle for bistatic angles is assumed to be the bisector of the angle between the transmitting and receiving antennas.

[1]Air Force Special Weapons Center, 6585th Test Group, Holloman Air Force Base, New Mexico, Radar Signature Measurements of BQM-34D and BQM-34F Target Drones, AFSWC-TR-74-01, January 1974.

[2]James W. Wright, On the Statistical Analysis of the Radar Signature of the MQM-34D, Interim Report Number One, US Army Missile Command, Redstone Arsenal, Alabama, Technical Report RE-75-7, 2 October 1974.

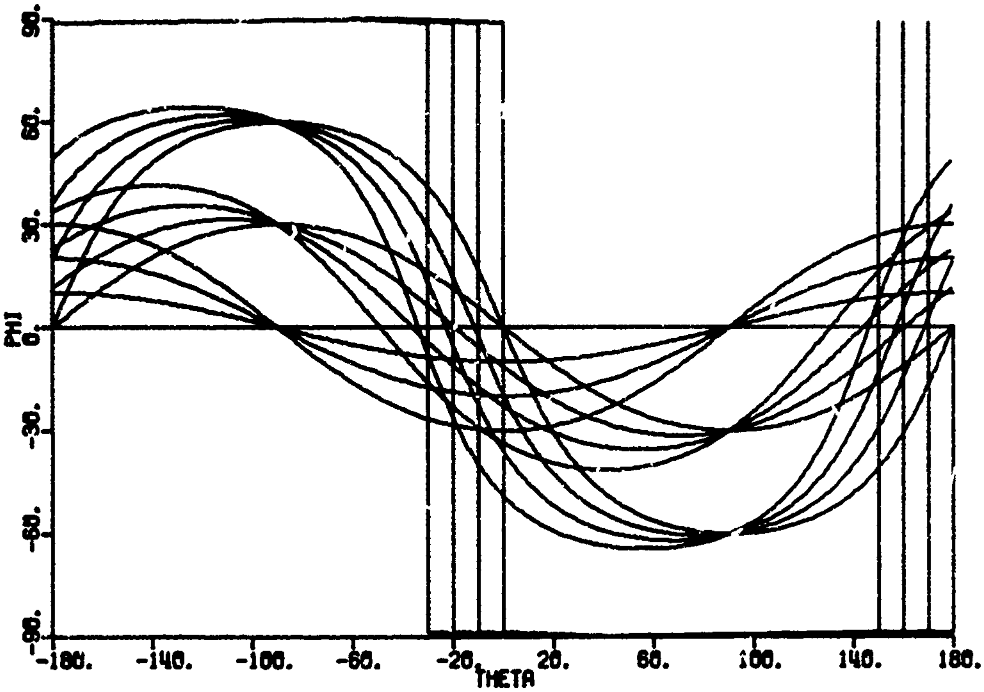

Figure 1. Aspect angles for the 16 data cuts.

Two sets of data are reported here. The first set is approximately all data within 15° of the normal to the roll axis (referred to also as broadside); the second set is all data within 30° of normal to the roll axis. Due to the differences in the measurement intervals, there are 10 times as many data points monostatically as bistatically. The data within 15° of broadside consist of 59,500 points monostatically and 5,950 points bistatically; the data within 30° of broadside consist of 122,500 data points monostatically and 12,250 data points bistatically.

It should be noted that for processing and storage efficiency the data were blocked in 2.5° sets. The selection process accepted all blocks of data for which the angle corresponding to the center of the block was within the specified limits and rejected all others. This process gives a stepped approximation to the ideal selection process.

Both sets of data include the aspect angle regions where the large specular reflections from the fuselage and aerodynamic surfaces are apparent. The large speculars are apparent for approximately ±5° from the normal to the roll axis, and decrease to small specular and refraction levels by approximately ±10° from the normal. The actual selection of the bounds for the two sets of data was essentially arbitrary.

DATA REDUCTION AND ANALYSIS

Each set of RCS data was processed to determine the average and standard deviation of the RCS in square meters (m^2) and in decibels referenced to one square meter (dBsm). Histogram type probability density functions and cumulative probability functions were computed for the measured data and three classical RCS models. The three classical RCS models were the Swerling 1 model, the Swerling 3 model, and the log-normal model.

The two Swerling RCS models were computed using the average and standard deviation of the RCS in m^2. The log-normal models were computed using the average and standard deviation of the RCS in dBsm. The values plotted for the RCS models were computed by numerically integrating the probability density functions over the appropriate intervals. The measured and computed probability functions were calculated and plotted on both linear and logarithmic scales. The measured data are plotted as a solid line, the Swerling 1 model with + symbols, the Swerling 3 model with x symbols, and the log-normal with ▷ symbols.

The glint data were processed to compute the average and standard deviation and compared to a normal distribution. The measured data are plotted as a solid line and the normal distribution with + symbols.

Table 1 summarizes the statistical quantities for each parameter for each condition, and Figure 2 presents the data on the RCS in graphical form. Unlike the data near nose-on, there is no apparent roll-off in the RCS for bistatic angles. This is approximately as one would expect for speculars from quadratic surfaces. The variations in the RCS as a function of bistatic angle are affected by variations in multiple reflections and shadowing (masking) which change as a function of bistatic angle.

Glint was measured at only two bistatic angles, 0° and 30°, so no curves appeared appropriate. It is noted, however, that the glint is reduced in standard deviation by approximately 4 dB at 30° bistatic angle.

Figures 3 and 4 present the curves comparing measured data and theoretical models for the two sets of data. For all conditions, the measured RCS data are best approximated by the log-normal model. The glint data are more difficult to describe for these sets of data than for the near nose-on cases. The distributions have larger concentrations of data near the average than the normal distribution, but have long tails. Monostatically, the standard deviation of glint is approximately one-half the target length, but 63% of the samples fall within approximately one-third of the target length of the average. Bistatically (30°), the glint appears to be much closer to a normal distribution, but the standard deviation is only about one-fourth of the target length.

CONCLUSIONS

The RCS in the aspect angle region near normal to the roll axis does not roll off with increasing bistatic angle, at least for bistatic angles less than 30°. The RCS in this region is dominated by the specular reflections from the fuselage and the aerodynamic surfaces which have large radii of curvature. Multiple reflections from these surfaces can also be rather large in these regions. The average value is affected by the limits selected for the computations since the large specular components are within approximately 5° of the normal. For the two sets of data presented here, the probability distributions are best approximated by the log-normal distribution.

The glint in the near broadside aspects is rather large. The standard deviation is approximately one-half of the target length monostatically and approximately one-fourth of the target length at 30° bistatic angle.

TABLE 1. SUMMARY OF STATISTICAL CHARACTERISTICS OF THE RADAR SIGNATURE OF THE MQM-34D NEAR NORMAL TO THE ROLL AXIS (VERTICAL POLARIZATION)

Parameter	Units	Bistatic Angle			
		0^{o}	10^{o}	20^{o}	30^{o}
		Within 15^{o} of Normal to Roll Axis			
Average of RCS	m^2	31.758	31.199	37.969	36.073
Std dev of RCS	m^2	78.120	75.861	106.010	81.251
Average of RCS	dBsm	8.842	8.746	8.715	9.628
Std dev of RCS	dBsm	8.054	8.012	8.324	7.741
Average of glint	ft	-2.215	-	-	-0.084
Std dev of glint	ft	15.806	-	-	6.154
		Within 30^{o} of Normal to Roll Axis			
Average of RCS	m^2	16.555	16.099	19.416	18.521
Std dev of RCS	m^2	56.533	54.961	76.131	59.239
Average of RCS	dBsm	3.201	2.709	2.537	3.252
Std dev of RCS	dBsm	9.322	9.550	9.909	9.702
Average of glint	ft	-1.196	-	-	-0.404
Std dev of glint	ft	13.096	-	-	5.611

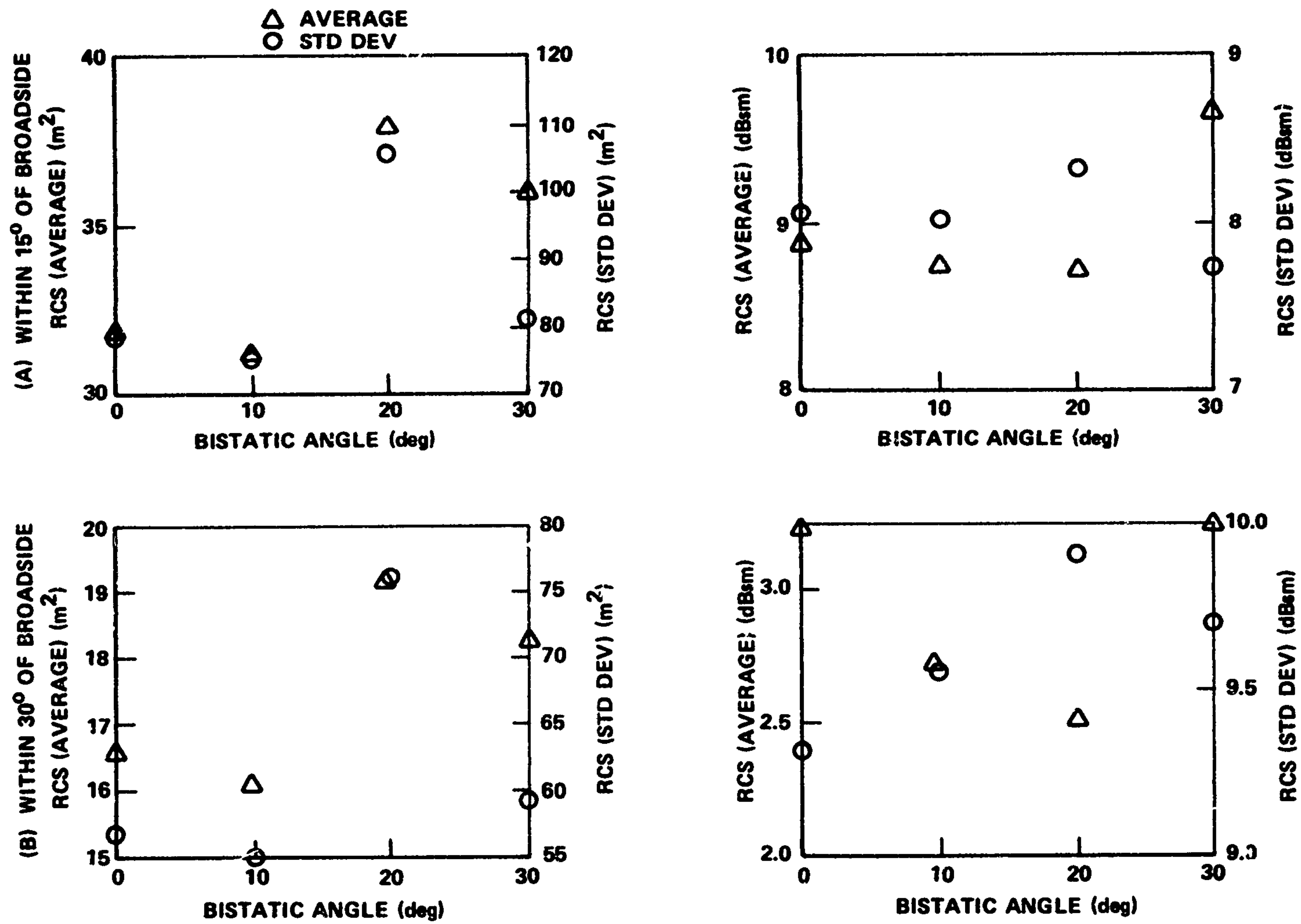

Figure 2. Statistical characteristics of the RCS as a function of bistatic angle.

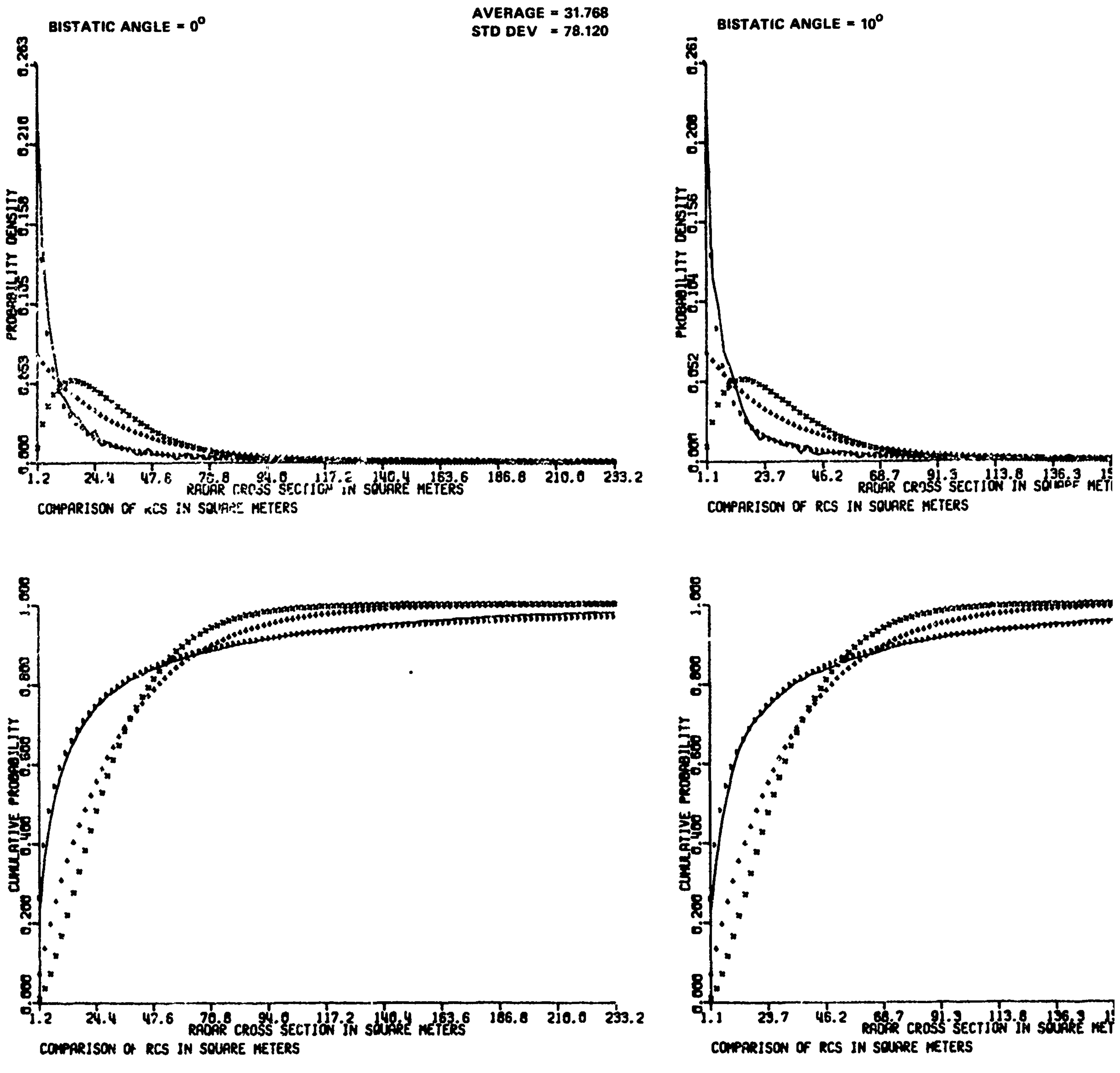

Figure 3. Comparison of theo

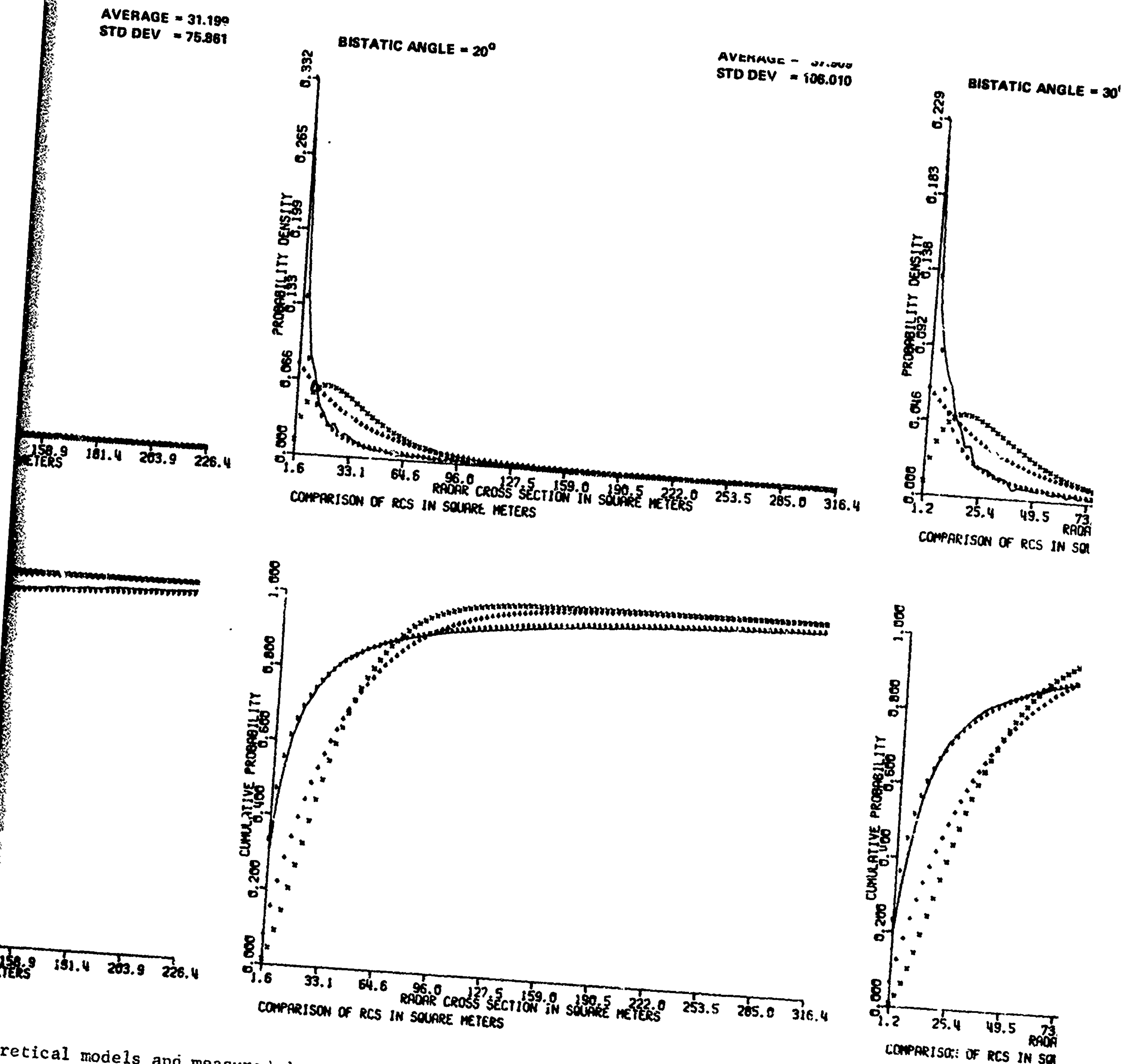

eoretical models and measured data within 15° of normal to the roll axis.

AVERAGE = 37.50
STD DEV = 106.010

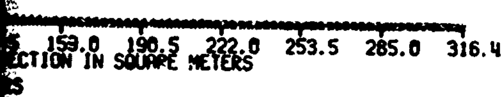

BISTATIC ANGLE = 30°

AVERAGE = 36.073
STD DEV = 81.251

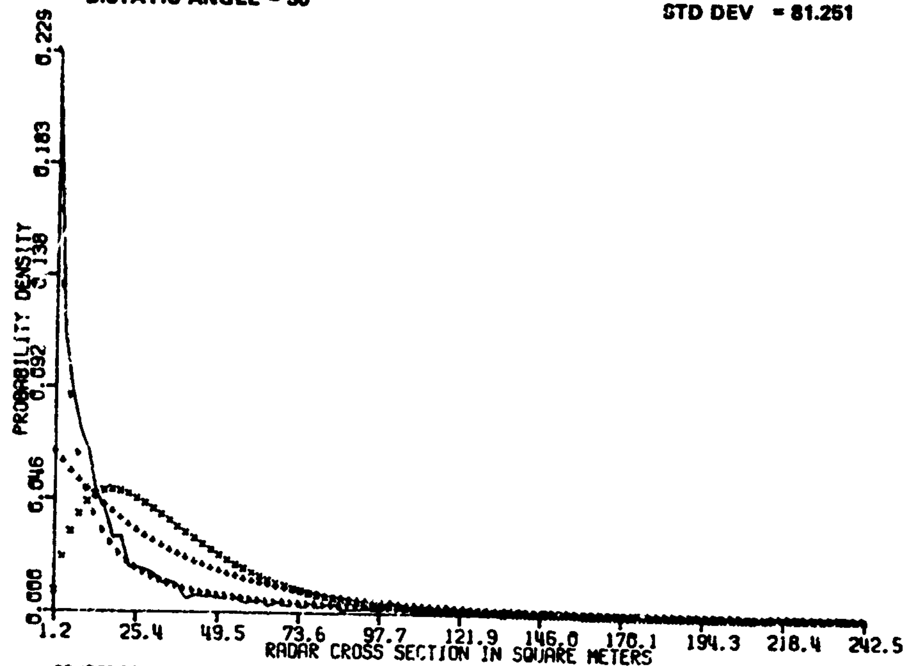

COMPARISON OF RCS IN SQUARE METERS

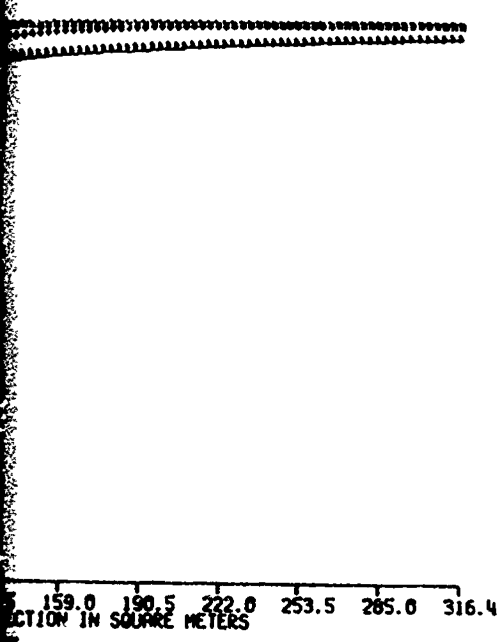

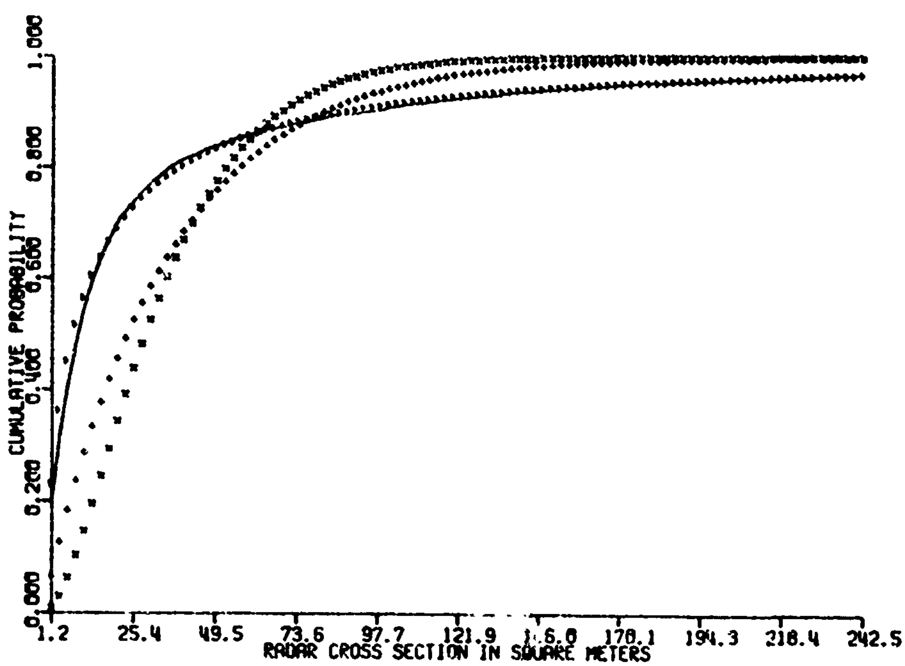

COMPARISON OF RCS IN SQUARE METERS

rmal to the roll axis.

BISTATIC ANGLE = 0°

AVERAGE = 8.842
STD DEV = 8.054

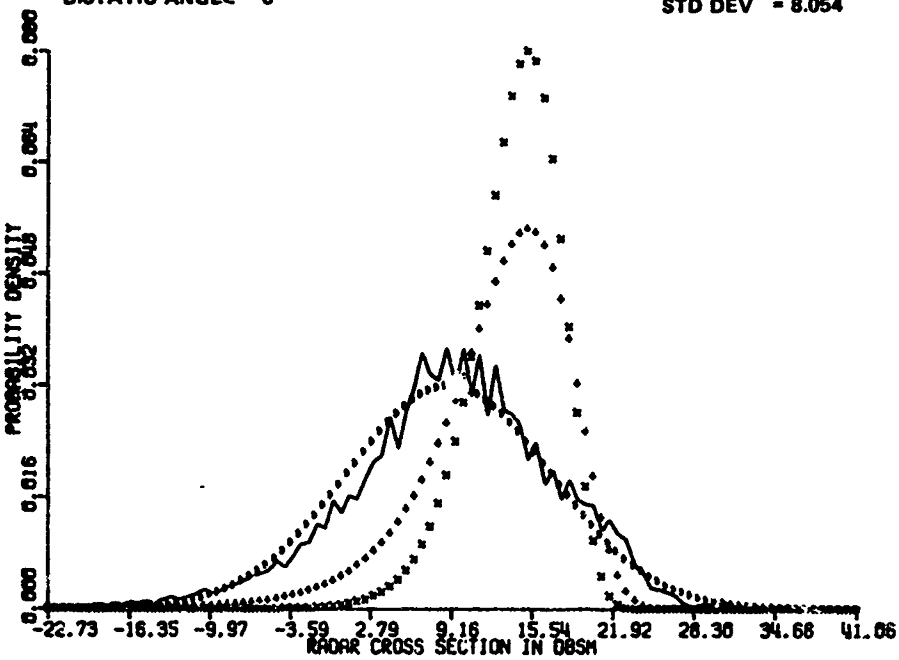

COMPARISON OF RCS IN DBSM

BISTATIC ANGLE = 10°

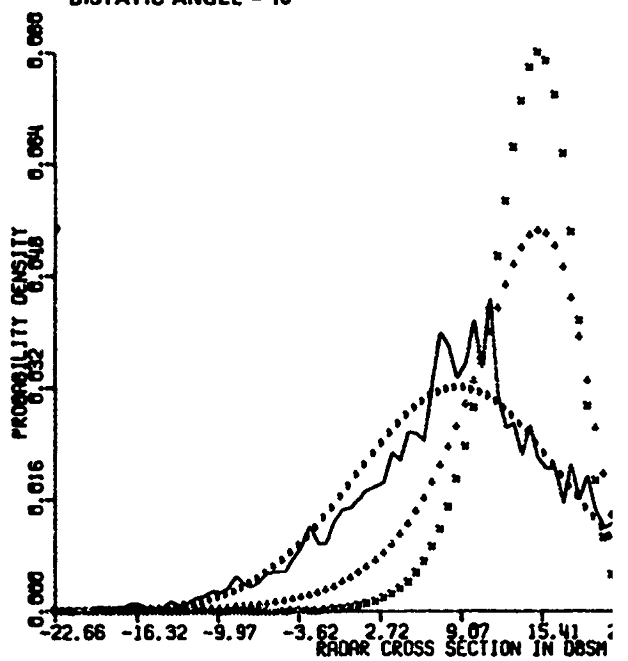

COMPARISON OF RCS IN DBSM

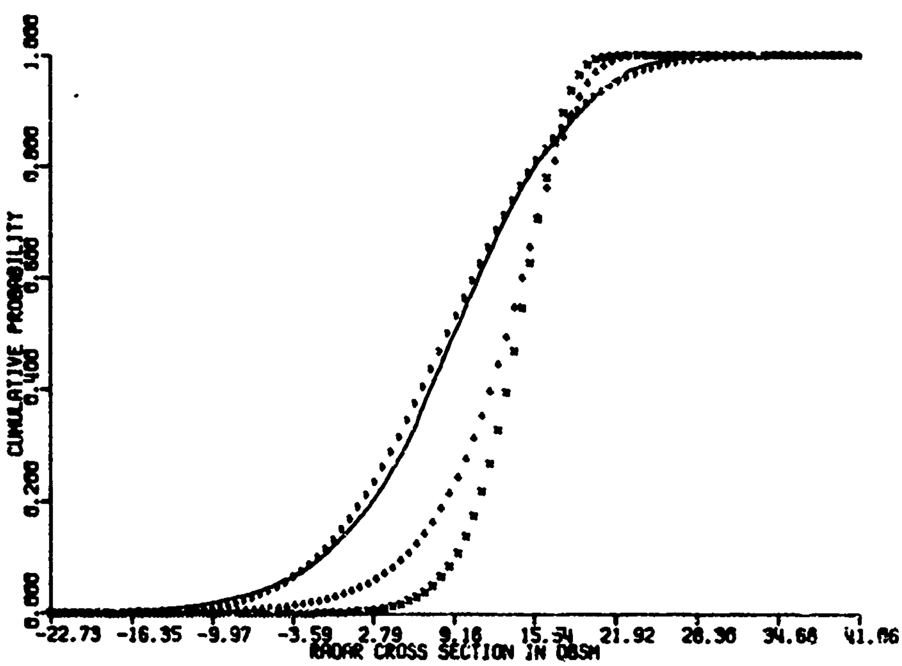

COMPARISON OF RCS IN DBSM

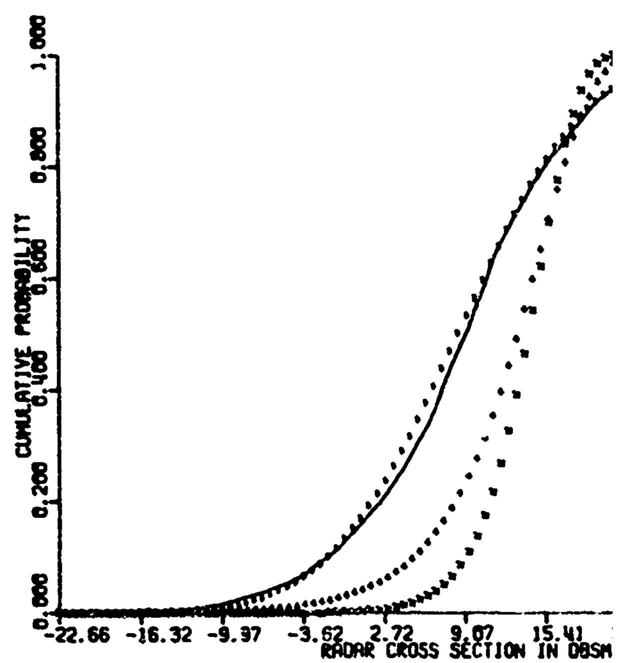

COMPARISON OF RCS IN DBSM

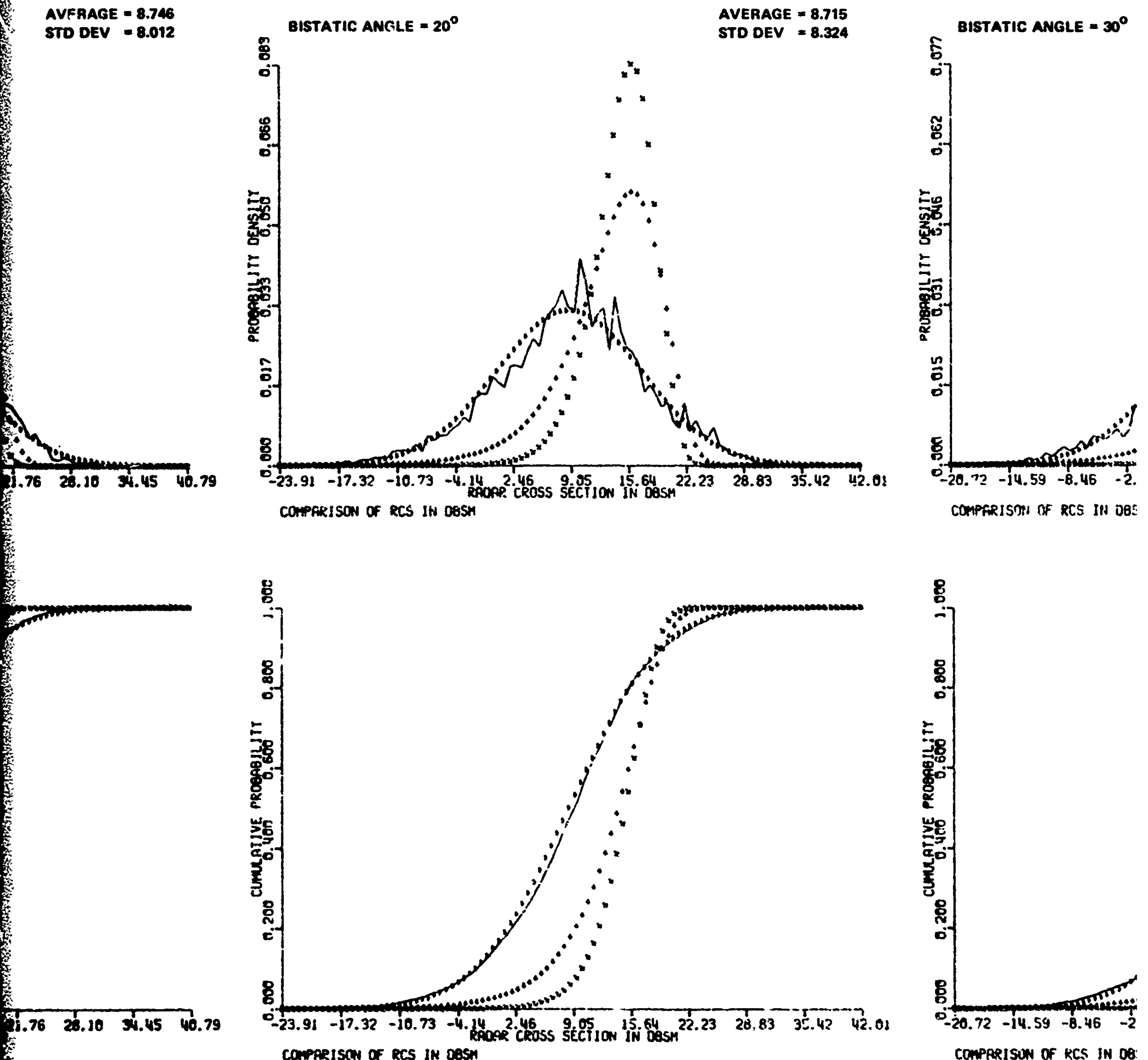

Figure 3. Continued.

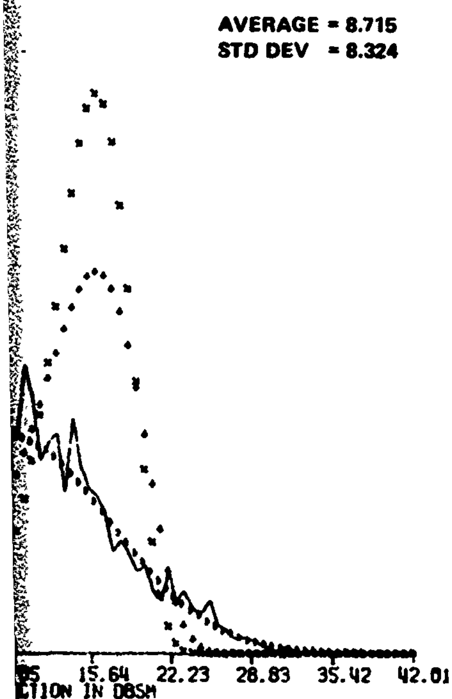

BISTATIC ANGLE = 30°

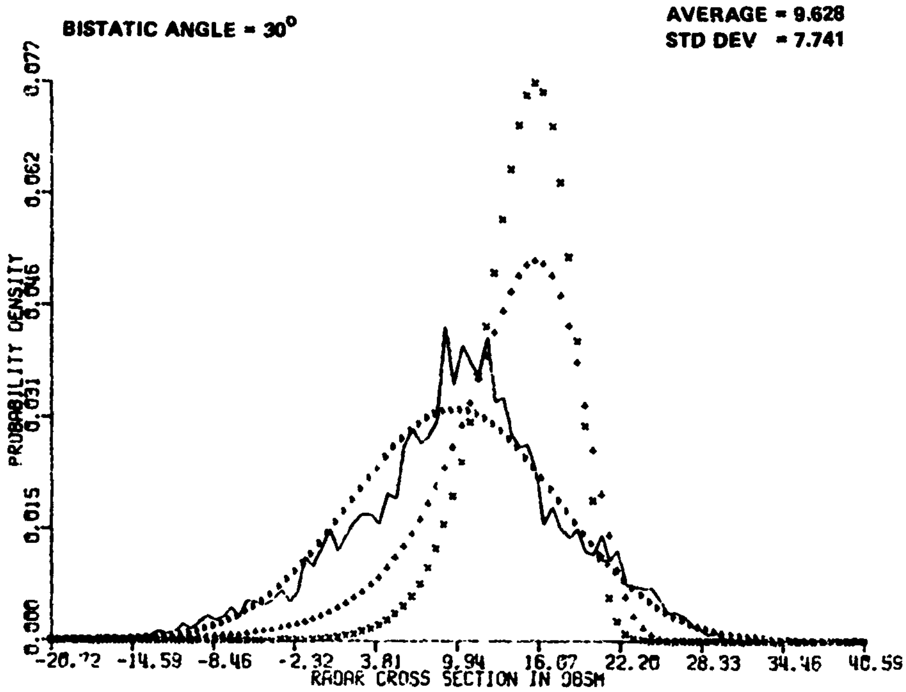

COMPARISON OF RCS IN DBSM

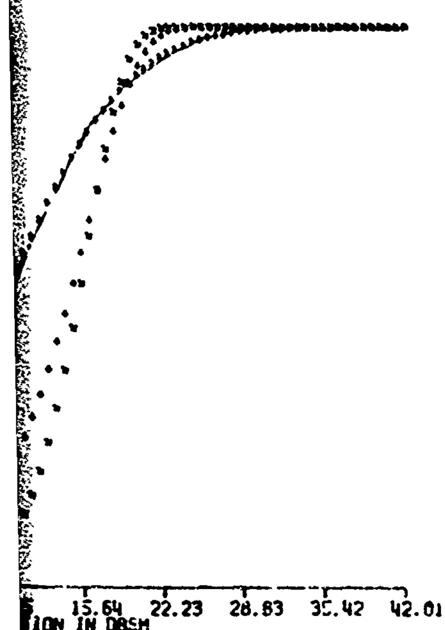

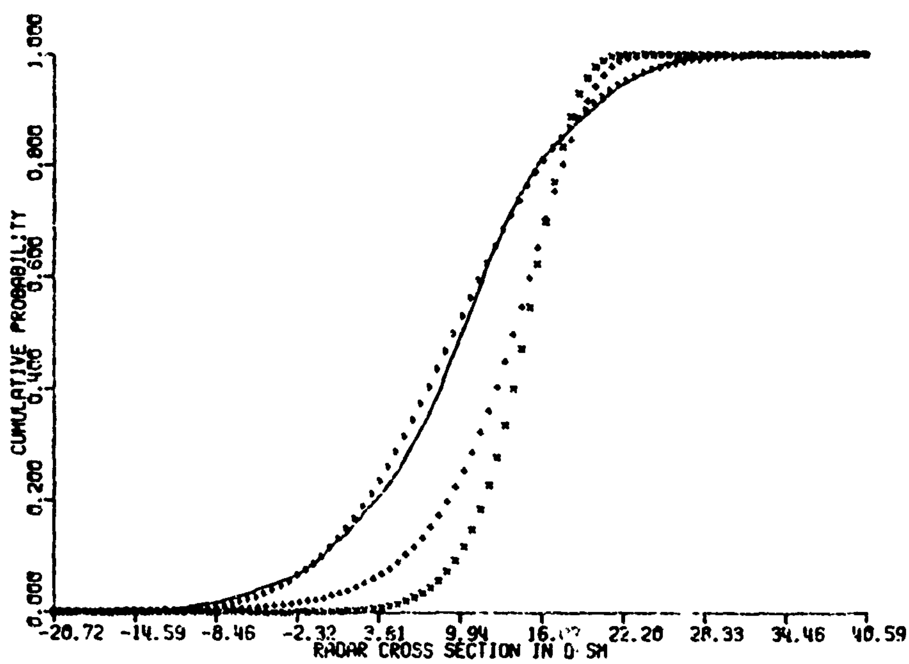

COMPARISON OF RCS IN DBSM

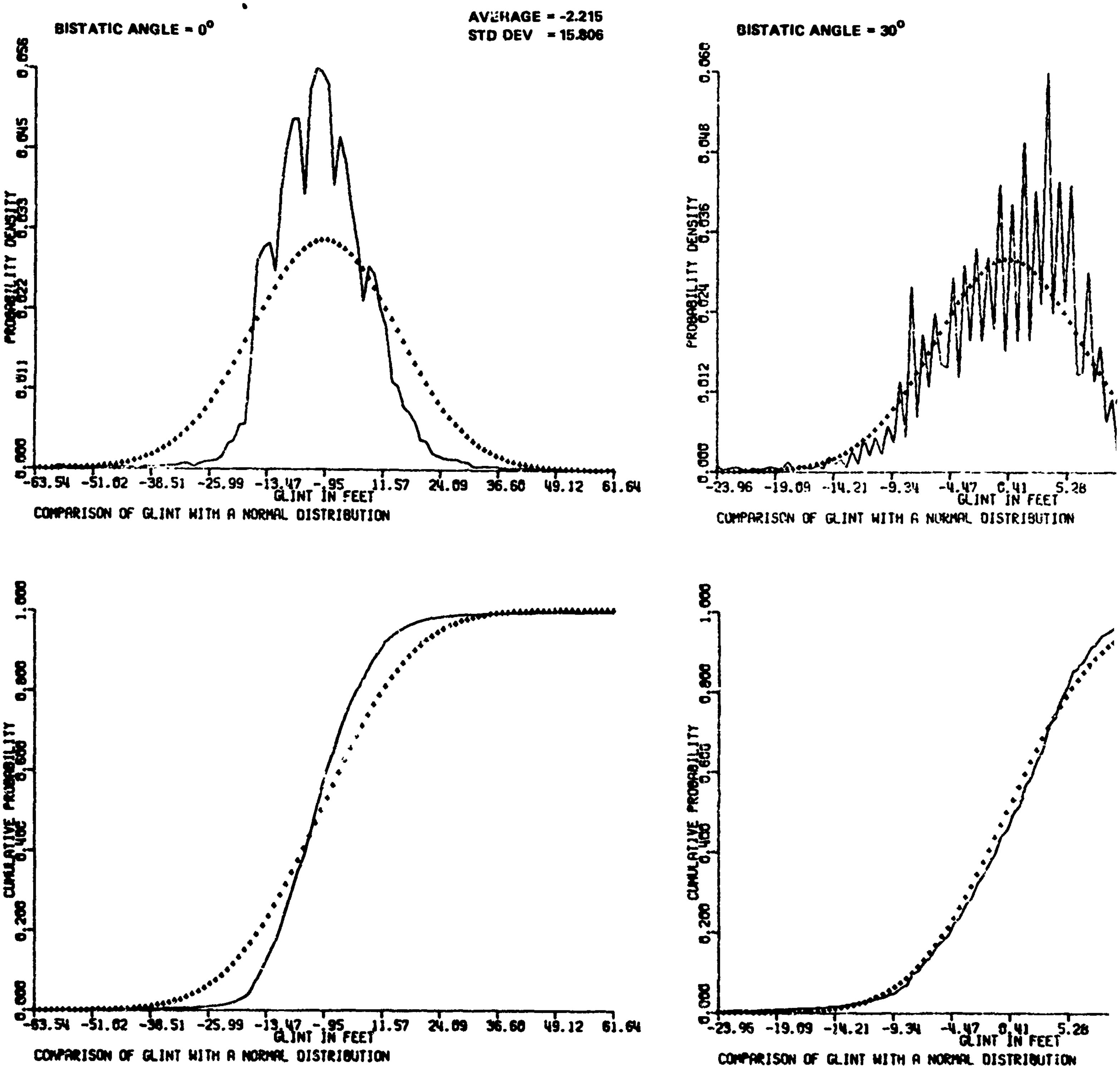

Figure 3. Concluded.

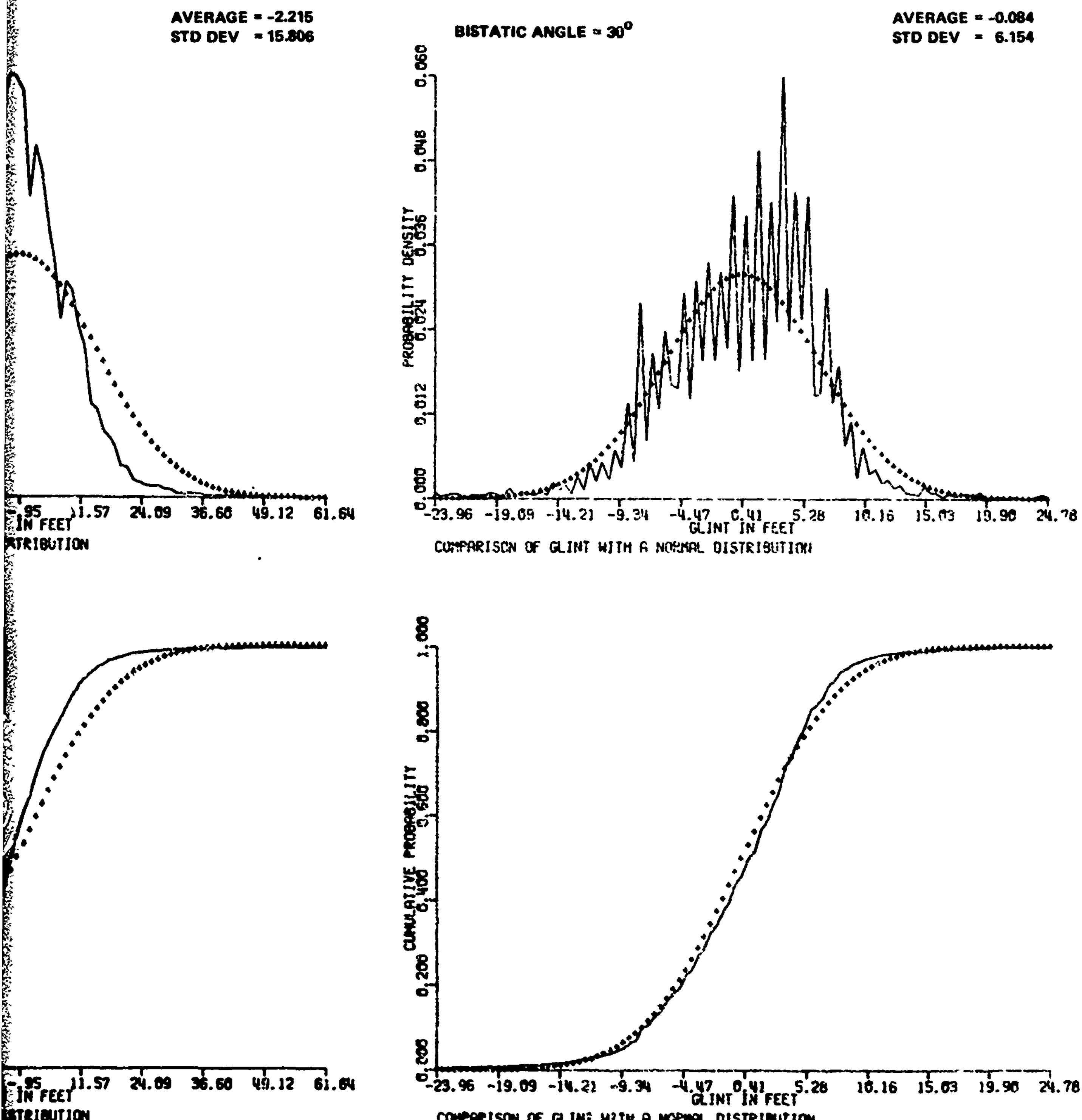

Figure 3. Concluded.

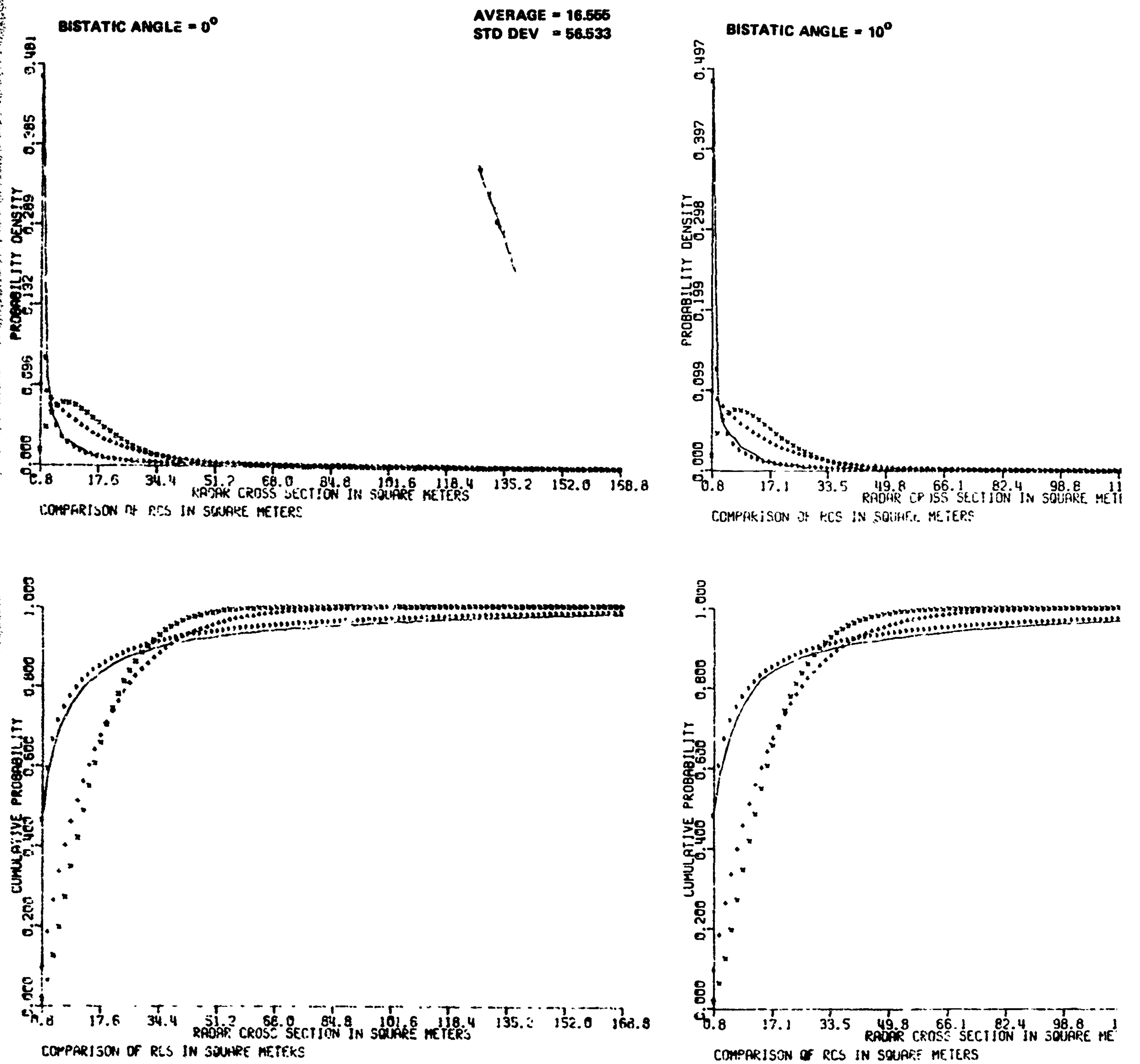

Figure 4. Comparison of theore

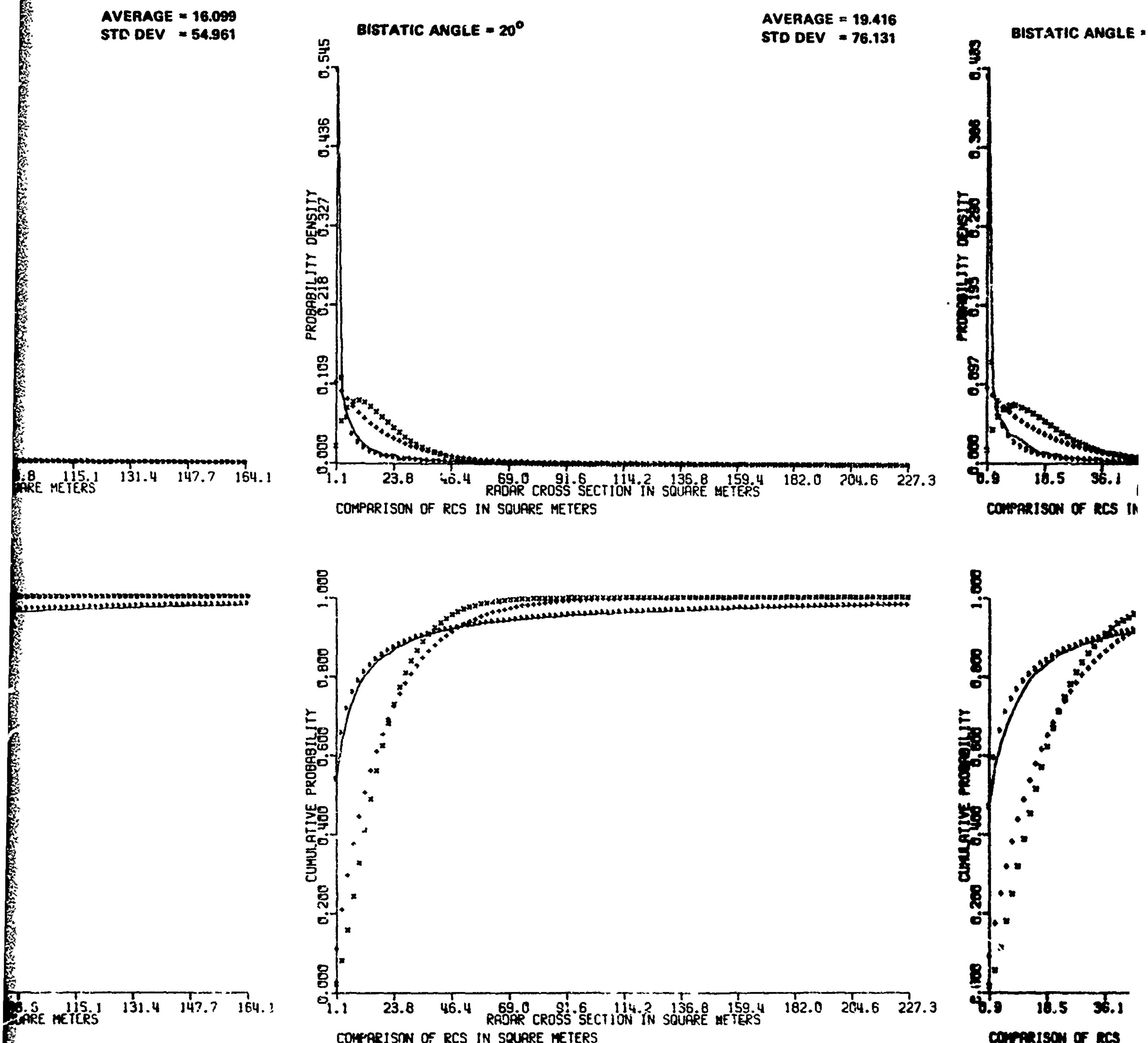

theoretical models and measured data within 30° of the normal to the roll axis.

AVERAGE = 19.416
STD DEV = 76.131

BISTATIC ANGLE = 30°

AVERAGE = 18.521
STD DEV = 59.239

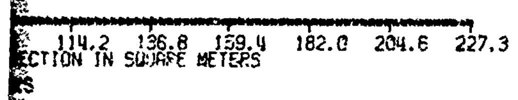

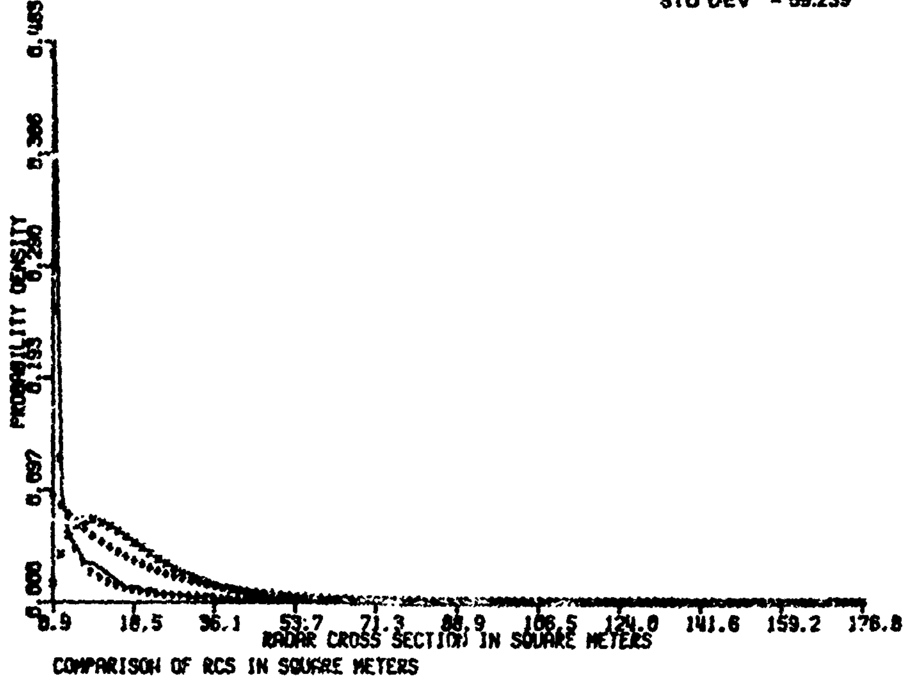

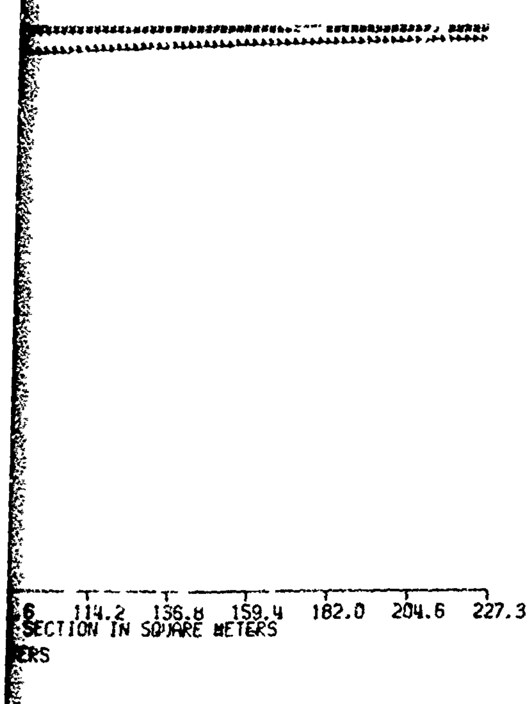

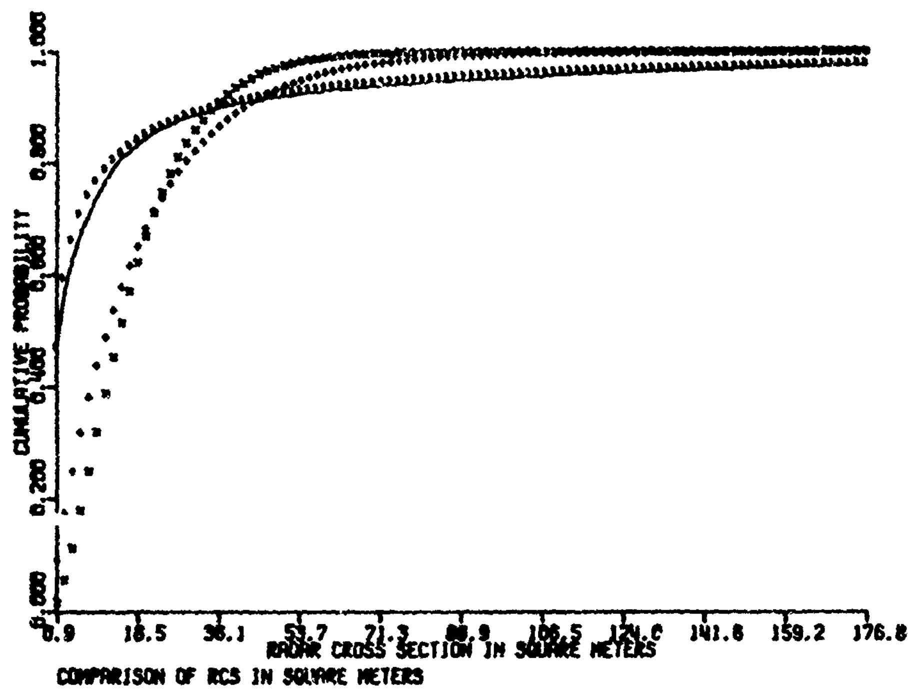

e normal to the roll axis.

BISTATIC ANGLE = 0°

AVERAGE = 3.201
STD DEV = 9.322

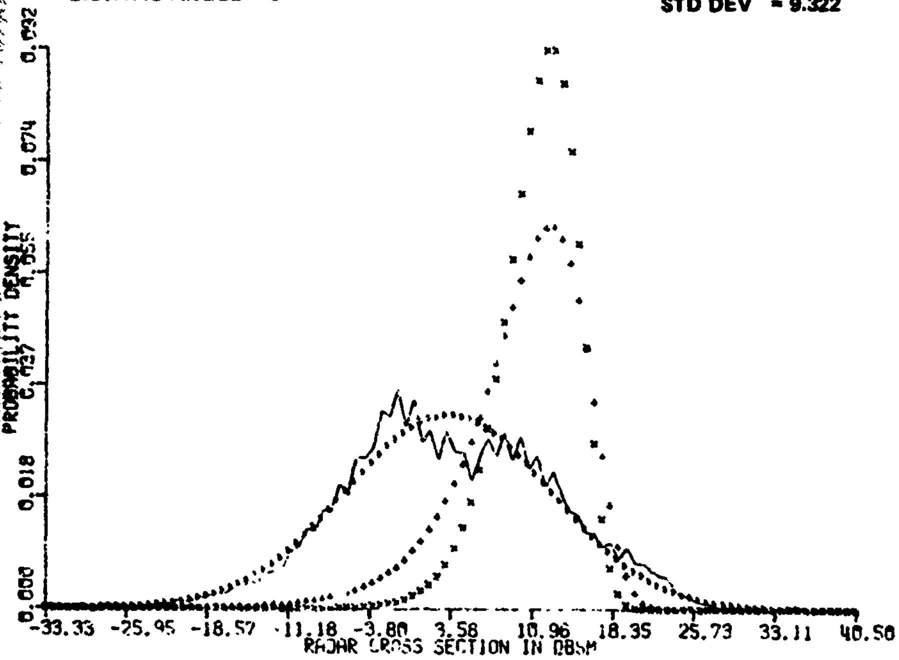

COMPARISON OF RCS IN DBSM

BISTATIC ANGLE = 10°

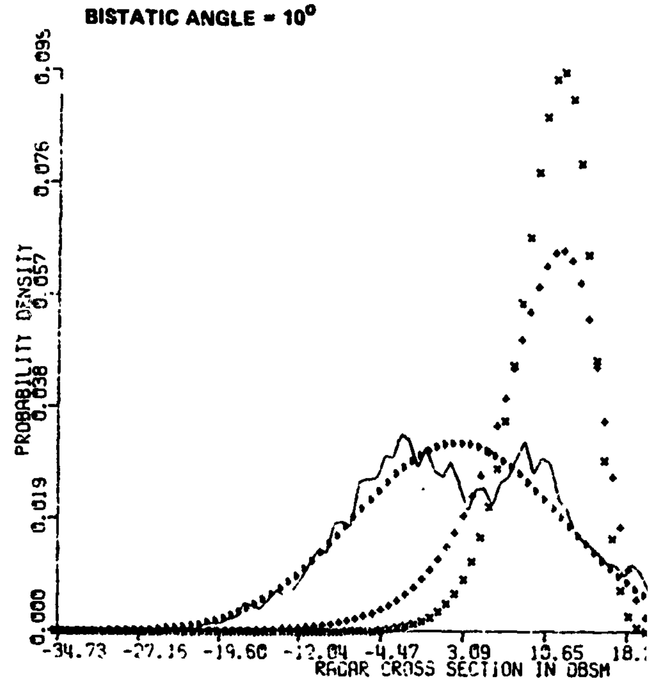

COMPARISON OF RCS IN DBSM

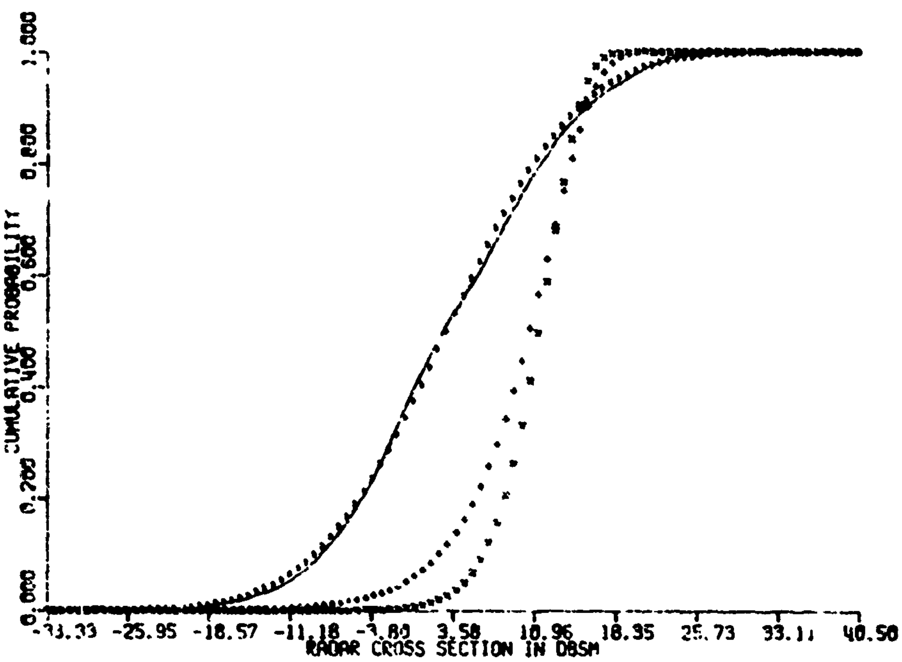

COMPARISON OF RCS IN DBSM

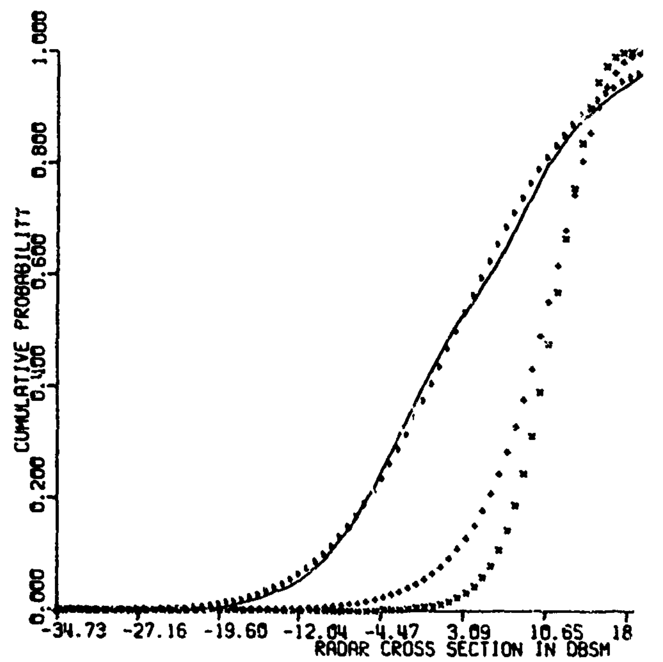

COMPARISON OF RCS IN DBSM

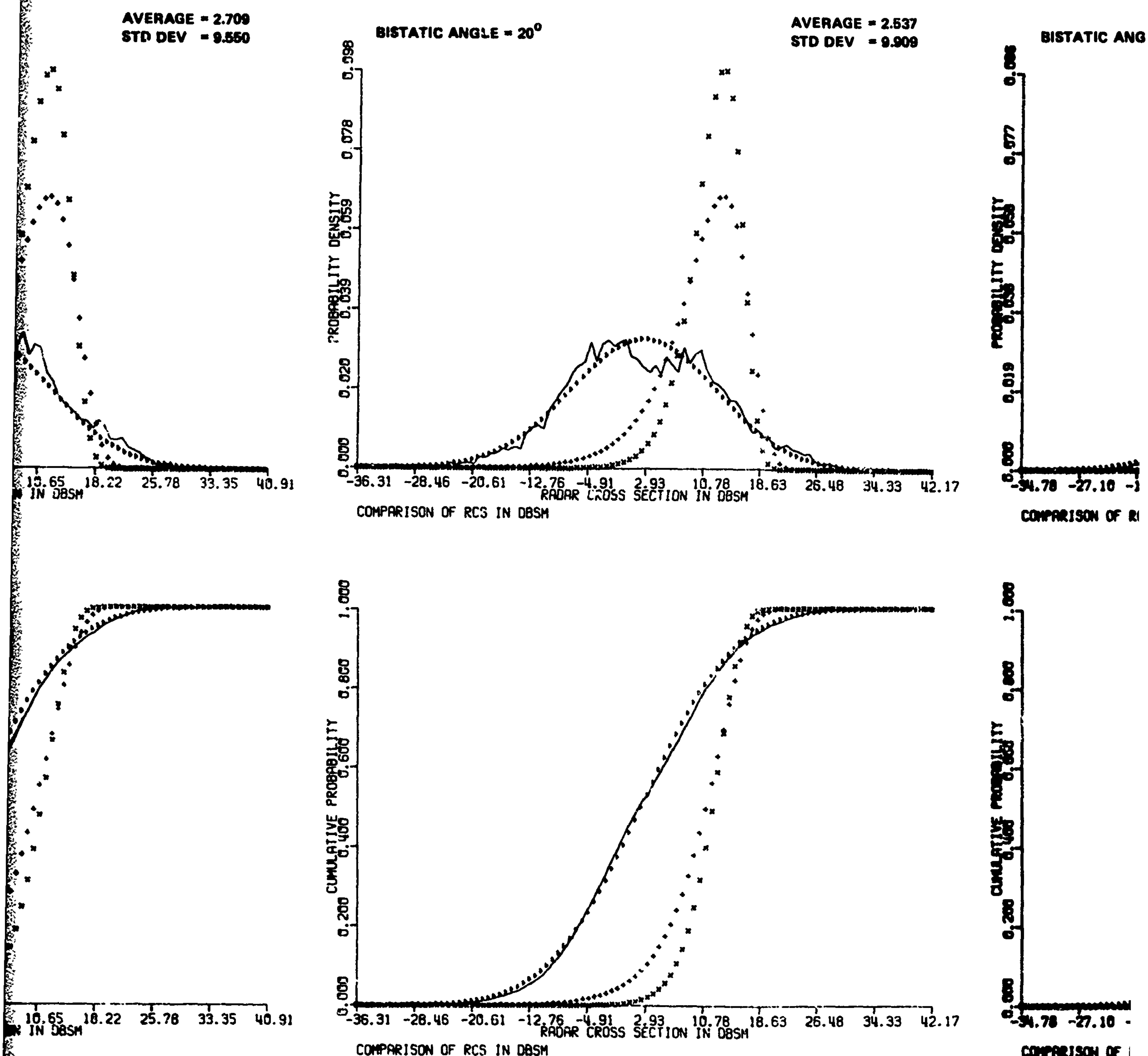

Figure 4. Continued.

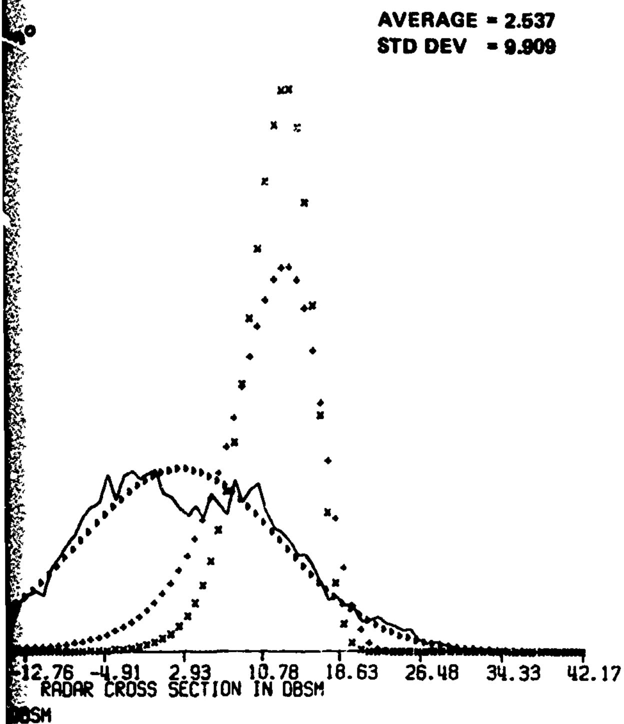

AVERAGE = 2.537
STD DEV = 9.909
-12.76 -4.91 2.93 10.78 18.63 26.48 34.33 42.17
RADAR CROSS SECTION IN DBSM
DBSM

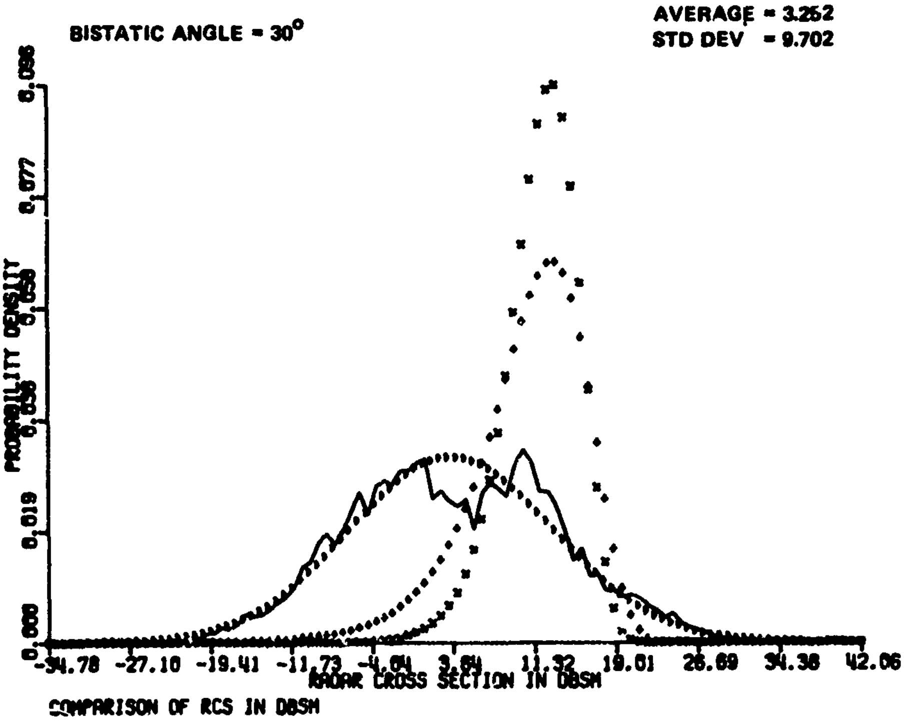

BISTATIC ANGLE = 30°
AVERAGE = 3.252
STD DEV = 9.702
PROBABILITY DENSITY
0.000 0.019 0.038 0.058 0.077 0.096
-34.78 -27.10 -19.41 -11.73 -4.04 3.64 11.32 19.01 26.69 34.38 42.06
RADAR CROSS SECTION IN DBSM
COMPARISON OF RCS IN DBSM

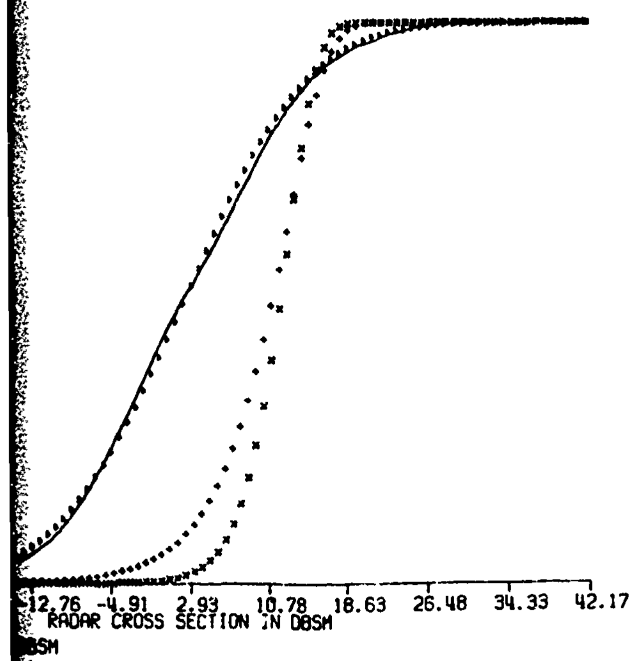

-12.76 -4.91 2.93 10.78 18.63 26.48 34.33 42.17
RADAR CROSS SECTION IN DBSM
DBSM

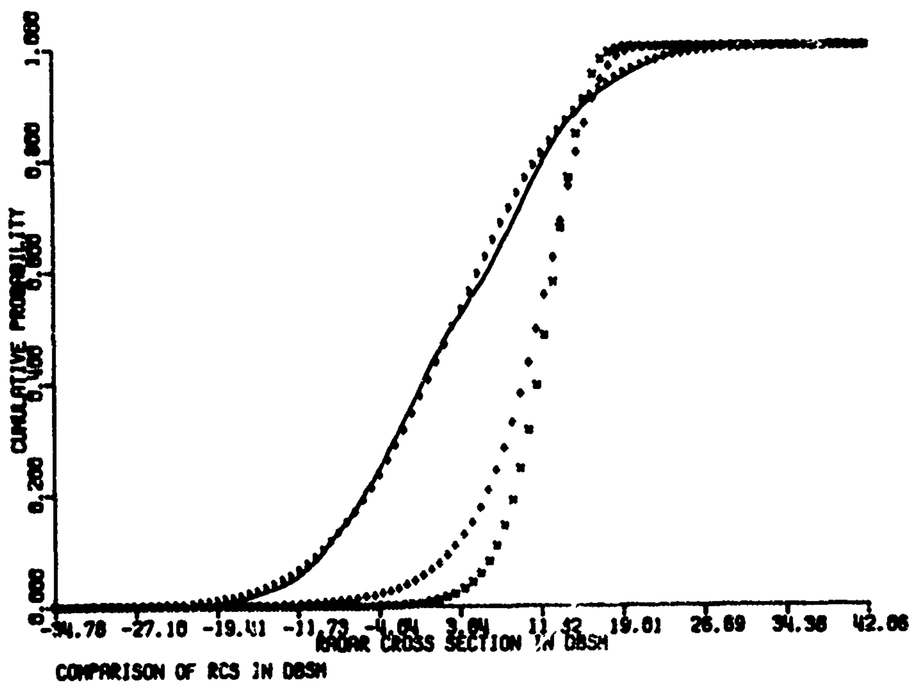

CUMULATIVE PROBABILITY
0.000 0.200 0.400 0.600 0.800 1.000
-34.78 -27.10 -19.41 -11.73 -4.04 3.64 11.32 19.01 26.69 34.38 42.06
RADAR CROSS SECTION IN DBSM
COMPARISON OF RCS IN DBSM

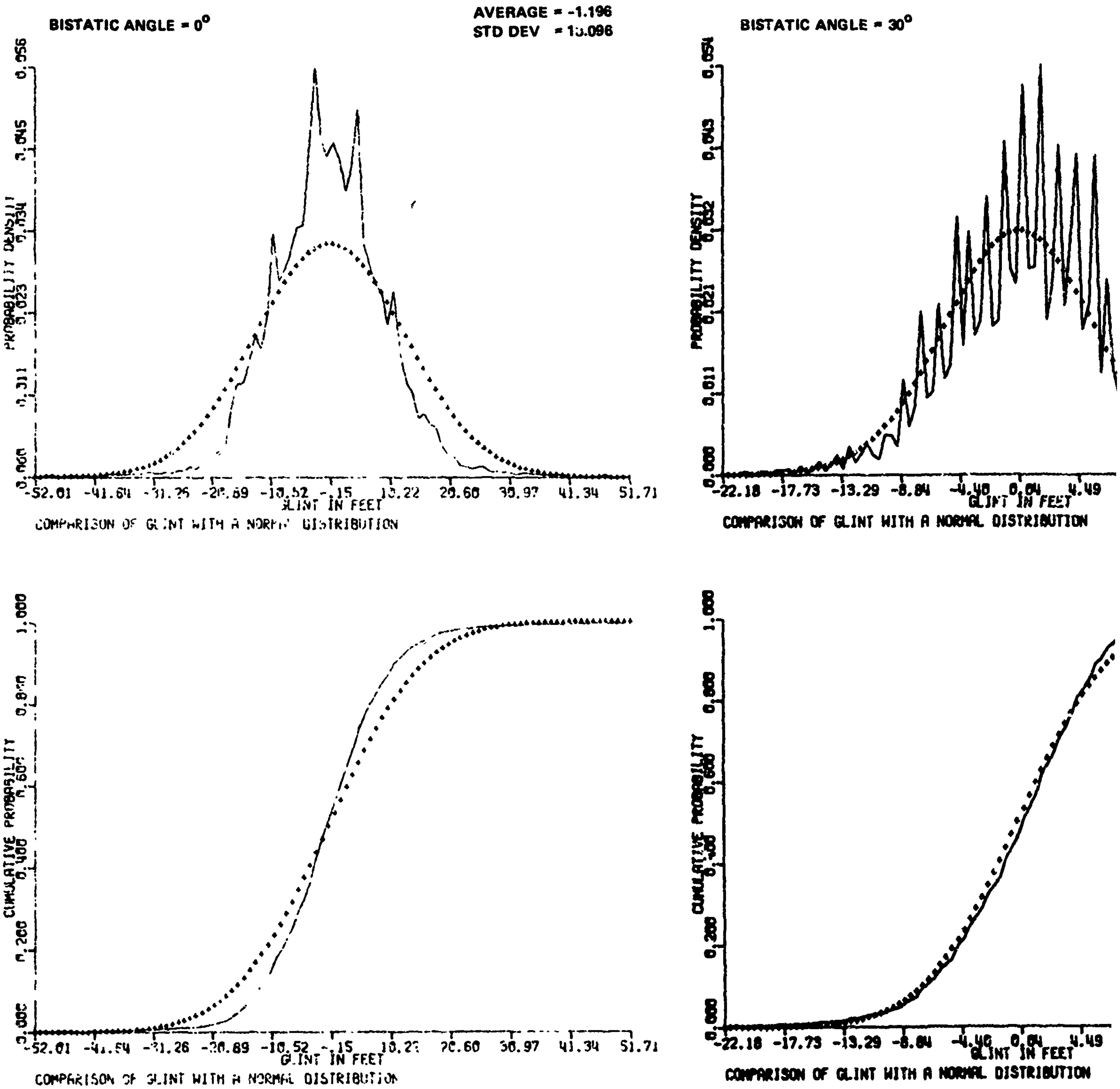

Figure 4. Concluded.

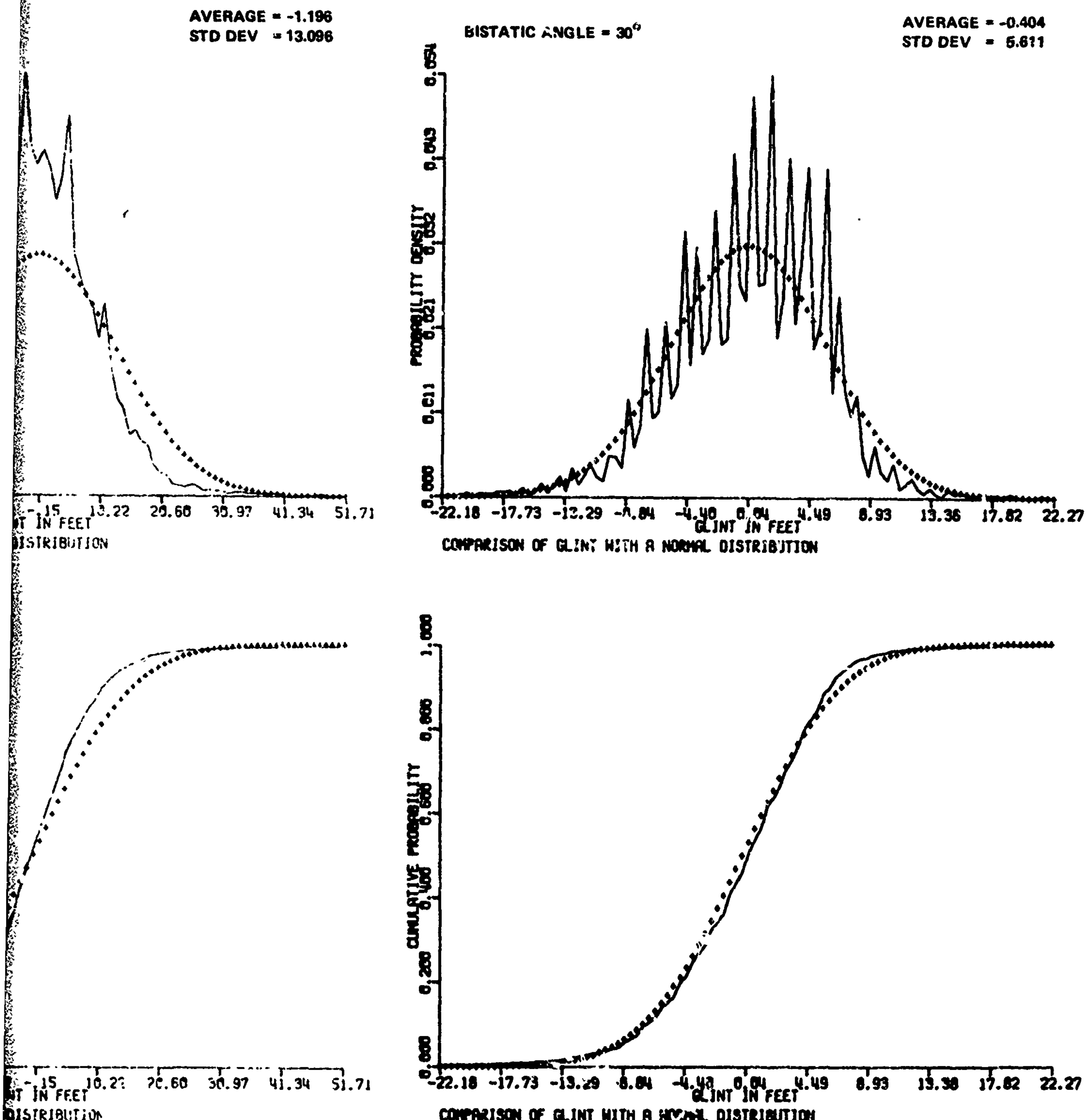

Figure 4. Concluded.